ELSEVIER

Materials Science and Engineering A 413–414 (2005) 555–560

MATERIALS SCIENCE & ENGINEERING A

www.elsevier.com/locate/msea

Development of creep resistant die cast Mg–Sn–Al–Si alloy

Dae H. Kang, Sung S. Park, Nack J. Kim *

Center for Advanced Aerospace Materials, Pohang University of Science and Technology, San 31, Hyoja-dong, Nam-gu, Pohang, Kyungbuk 790-784, Republic of Korea

Abstract

A study has been made on the tensile properties and high temperature properties of die cast Mg–Sn–Al–Si (TAS831) alloy. The microstructure of TAS831 alloy is characterized by the presence of thermally stable Mg_2Sn particles within matrix and along grain boundaries. It also contains a small volume fraction of thermally stable Mg_2Si particles. It has been shown that TAS831 alloy has better combinations of tensile properties at room and elevated temperatures than die cast AZ91 alloy. Creep properties of TAS831 alloy are also superior to those of AZ91 alloy. Analyses of creep behavior and load-relaxation behavior at elevated temperatures in the context of internal variable theory indicate that the presence of thermally stable dispersoids in TAS831 alloy increases the resistance to dislocation movement, thereby improving creep properties over those of AZ91 alloy.

Keywords: Mg–Sn alloy; Dispersoid; Creep resistance; Load-relaxation test

1. Introduction

Mg alloys have the great potential for high performance structural applications due to their excellent properties such as low density, high specific strength, superior damping capacity, etc. [1,2]. In addition, these alloys usually have good castability and machinability, making them quite suitable for applications as casting alloys. The typical alloys are Mg–Al based alloys such as AZ91 and AM60 alloys. They are currently used extensively in automotive components such as instrument panel, intake manifold and steering wheel to name a few [3,4]. However, Mg–Al based alloys are unsuitable for use at temperatures above 120 °C since they show poor creep resistance and large decrease in strength at elevated temperatures due to the thermal instability of microstructure [5,6]. Therefore, in recent years, improving the elevated temperature properties has become a major issue for possible applications of Mg alloys in hot components such as powertrain systems. Several approaches have been taken to improve the elevated temperature properties of Mg alloys [6–14]. The most common way of improving the elevated temperature properties is the formation of thermally stable precipitates or dispersoids along the grain boundaries to resist the deformation by grain boundary sliding [12]. The most effective alloying elements for such purpose are rare earth elements, which result in a significant improvement in the elevated temperature properties [13]. However, these elements are expensive, limiting widespread application of such alloys.

In the present paper, an alternative alloy based on Mg–Sn system, TAS831 alloy (Mg–8Sn–3Al–1Si), is introduced. Sn has several characteristics suitable as an alloying element for elevated temperature applications: low diffusivity in Mg (10×10^{-14} m/s^2 at 400 °C), low solid solubility in Mg (0.035 at.% at room temperature) and high liquid solubility in molten Mg (100% at 800 °C). Moreover, the main phase in Mg–Sn alloy system, Mg_2Sn, has a high melting temperature of about 770 °C. These characteristics suggest that a fairly large volume fraction of thermally stable Mg_2Sn particles can be formed during solidification. Tensile and creep properties of die cast TAS831 alloy were investigated and compared to those of die cast AZ91 alloy. Load-relaxation behavior of these alloys was also investigated to understand the elevated temperature deformation mechanism.

2. Experimental procedures

TAS831 and AZ91 alloys were subjected to die casting. The analyzed chemical compositions are Mg–7.79 wt.% Sn–2.73 wt.% Al–0.70 wt.% Si–0.69 wt.% Zn–0.19 wt.% Mn for TAS831 alloy and Mg–9.2 wt.% Al–0.85 wt.% Zn–0.21 wt.% Mn for AZ91 alloy. Al was added to TAS831 alloy for increasing the castability. Si was also added to TAS831

* Corresponding author. Tel.: +82 54 279 5135; fax: +82 54 279 5887.
E-mail address: njkim@postech.ac.kr (N.J. Kim).

0921-5093/$ – see front matter © 2005 Elsevier B.V. All rights reserved.
doi:10.1016/j.msea.2005.09.022

alloy to utilize the thermally stable Mg_2Si phase, which is known to improve the creep resistance of Mg alloys [4,6,9–11]. The alloys were melted at 680 °C under an inert atmosphere of CO_2 and SF_6 mixture. The melt was injected into the mold with the applied die pressure of 260 kg/cm^2. The mold temperature was 200 °C. Tensile properties were measured by using flat tensile specimens with 12.6 mm gauge length, 1 mm gauge thickness and 5 mm gauge width at a strain rate of $6.4 \times 10^{-4}\,s^{-1}$. High temperature creep tests were performed in a horizontal creep tester at 150 °C with loads of 50 MPa and 75 MPa. Creep specimens were cylindrical ones with gauge length of 24.0 mm and gauge diameter of 5 mm. High temperature load-relaxation tests were conducted using a computer controlled electro-mechanical testing machine (Instron 1361 model) equipped with a high temperature furnace capable of maintaining temperature fluctuation within ±0.5 K. Cylindrical specimens with the dimensions of 24.0 mm gauge length and 5 mm gauge diameter were tested at 150 °C and 250 °C.

3. Results and discussion

3.1. Microstructure and tensile properties

Fig. 1 shows the scanning electron microscopy (SEM) images of die cast AZ91 and TAS831 alloys. The characteristic features of microstructures of these alloys can be described as follows. In AZ91 alloy, continuous network of $Mg_{17}Al_{12}$ particles (10.8 vol.%) is observed along grain boundaries (Fig. 1a). On the other hand, semi-continuous grain boundary particles (10.3 vol.%) are observed for die cast TAS831 alloy as shown in Fig. 1b. Transmission electron microscopy (TEM) analysis of grain boundary particles shows that they consist mostly of Mg_2Sn phase as shown in Fig. 2a. Small amounts of $Mg_{17}Al_{12}$ and Mg_2Si particles are also observed. It is interesting to note that Mg_2Si particles are present as globular particles in the present alloy. The more common morphology of Mg_2Si phase is the Chinese-script one, which forms under slow cooling conditions and is quite detrimental to the tensile properties of Mg alloys [15]. The fast cooling rate of die casting process prevents the formation of Chinese-script Mg_2Si particles. Besides the grain boundary particles, there are also fine (<50 nm) particles within the matrix of TAS831 alloy (Fig. 2b). Analysis of SAD pattern shows that these particles are Mg_2Sn particles, which have no orientation relationship with Mg matrix. The above-mentioned differences in the microstructural features between AZ91 and TAS831 alloys such as the types of grain boundary phases and the presence of second phase in matrix will affect the tensile and creep properties differently.

Tensile properties of the alloys at various temperatures are shown in Table 1. At room temperature, tensile properties of AZ91 alloy are quite similar to those of TAS831 alloy, except ductility. Higher ductility of TAS831 alloy than that of AZ91 alloy can be ascribed to the semi-continuous morphology of grain boundary particles of TAS831 alloy and also to the presence of fine Mg_2Sn particles in the matrix of TAS831 alloy, which induce the Orowan bypassing of dislocations. It has been shown that AZ91 alloy fails by intergranular fracture due to the continuous network of $Mg_{17}Al_{12}$ particles along grain boundaries [16]. With increase in test temperature, there is a decrease in strength for both alloys as expected. However, the degree of the decrease in strength with increase in temperature is smaller in TAS831 alloy than in AZ91 alloy, indicating the higher thermal stability of TAS831 alloy. This is mainly due to the presence of thermally stable Mg_2Sn particles within matrix and along grain boundaries in TAS831 alloy. Mg_2Si particles along grain boundaries are also expected to improve the high temperature tensile

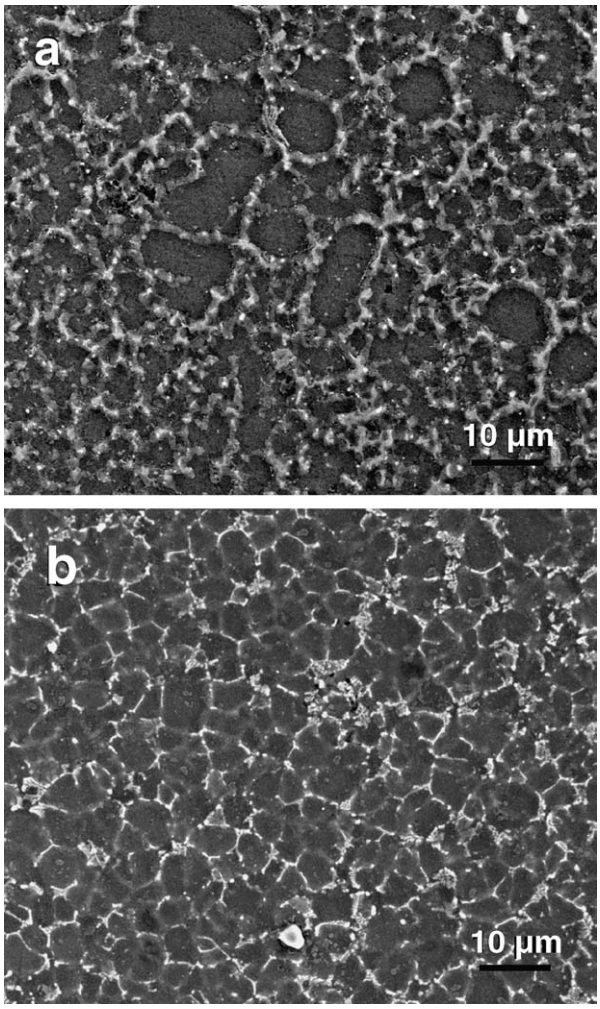

Fig. 1. SEM images of die cast (a) AZ91 and (b) TAS831 alloys.

Table 1
Tensile properties of die cast AZ91 and TAS831 alloys at various temperatures

Alloy	Temperature (°C)	YS (MPa)	UTS (MPa)	El. (%)
AZ91	Room temperature	166	210	2.0
	150	106	135	6.5
	200	92	106	10.8
	250	60	67	16.1
TAS831	Room temperature	162	207	4.1
	150	115	131	6.8
	200	96	102	9.2
	250	67	74	12.6

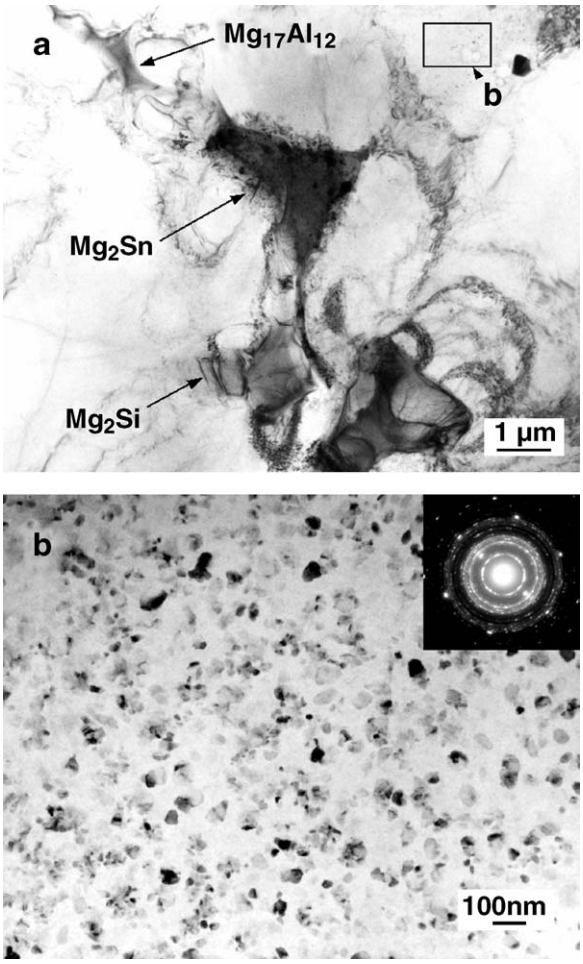

Fig. 2. TEM images of (a) grain boundary area and (b) matrix of die cast TAS831 alloy.

properties. Analysis of the microstructure after high temperature tensile tests shows that there is no change in the size and volume fraction of Mg_2Sn particles after high temperature exposure, indicating the superior thermal stability of Mg_2Sn phase.

3.2. Creep behavior

Creep properties of the alloys are summarized in Fig. 3. When tested at 150 °C with an applied stress of 50 MPa, TAS831 alloy shows a minimum creep rate more than 10 times lower than that of AZ91 alloy. Minimum creep rates of these alloys increase substantially as the applied stress increases from 50 MPa to 75 MPa; however, the minimum creep rate of the TAS831 alloy is still much lower than that of the AZ91 alloy. In fact, the creep resistance of the die cast TAS831 alloy is equivalent to those of the commercial creep resistant alloys [17].

In order to understand the detailed creep mechanism for the alloys, stress exponent (n) and activation energy (Q) were calculated. The minimum creep rate ($\dot{\varepsilon}$) is related to the applied stress and temperature by means of the conventional equation [18,19]

$$\dot{\varepsilon} = A\frac{D_0 G b}{kT}\left(\frac{\sigma}{G}\right)^n \exp\left(-\frac{Q}{RT}\right) \quad (1)$$

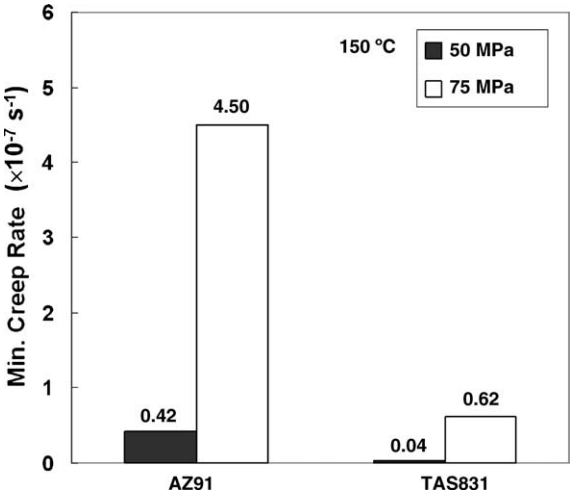

Fig. 3. Minimum creep rates of die cast AZ91 and TAS831 alloys.

where k is the Boltzmann's constant, b the length of the Burgers vector, D_0 a frequency factor, σ the applied stress and R is the gas constant. n and Q are parameters of the material that could give useful information on the creep controlling mechanisms. By plotting logarithmically the minimum creep strain rate $\dot{\varepsilon}$ versus the applied stress σ, we can calculate stress exponent, n. Plot of $\log \dot{\varepsilon}$ versus $1/T$ will yield the apparent activation energy Q. Table 2 shows the values of stress exponent and activation energy for both alloys. It shows that the stress exponent and activation energies of AZ91 alloy are calculated to be 2.9 kJ/mol and 114.5 kJ/mol, respectively. These values can be used to infer the dominant creep mechanisms for the alloy at the present test conditions. The stress exponent $n \cong 2$ is generally reported for grain boundary sliding, while $n = 4$–6 is for dislocation climb controlled creep [20]. Comparisons with the values of stress exponent reported in the literatures suggest that the dominant creep mechanism for the present AZ91 alloy is the grain boundary sliding. However, consideration of activation energy gives some confusing result. The activation energy $Q = 114.5$ kJ/mol is higher than the activation energies for grain boundary diffusion (92 kJ/mol) or cross slip (100 kJ/mol) usually observed for the Mg alloys deformed by grain boundary sliding. However, it is lower than the activation energy for lattice self-diffusion of Mg (135 kJ/mol) observed for the Mg alloys deformed by dislocation climb. In fact, there are some conflicting results on the creep mechanism of die cast AZ91 alloy [20]. For example, Regev et al. [12] reported the stress exponent of 6.9 when tested at 150 °C with applied stress ranging from 40 MPa to 100 MPa and proposed the dislocation climb controlled creep as the dominant creep mechanism. On the other hand, Dargusch et

Table 2
Values of stress exponent and activation energy for creep of die cast AZ91 and TAS831 alloys

Alloy	Stress exponent (n)	Activation energy (Q, kJ/mol)
AZ91	2.9	114.5
TAS831	6.9	132.9

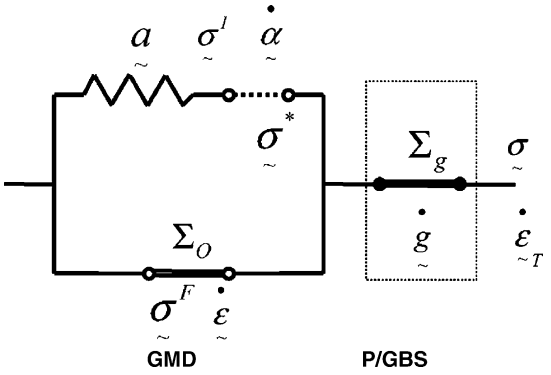

Fig. 4. Rheological model of an internal variable theory (GMD: grain matrix deformation and GBS: grain boundary sliding).

al. [21] showed that the stress exponent is approximately 2 at low stresses (20–40 MPa) and 5 at higher stresses (40–80 MPa) when at tested at 150 °C. These results indicate that creep of Mg alloys can occur by various mechanisms depending on several factors such as microstructure, stress and temperature regimes, and of course the alloy system. It can be seen in Table 2 that TAS831 alloy has larger values of stress exponent and activation energy than AZ91 alloy. The values of both parameters fit with the values for dislocation climb controlled creep, suggesting that the creep of TAS831 alloy occurs by dislocation climb controlled creep. The presence of thermally stable Mg_2Sn and Mg_2Si particles along grain boundaries pin grain boundaries and hinder both grain boundary migration and sliding during high temperature exposure. The presence of fine Mg_2Sn particles within matrix also contributes to the improved creep resistance of TAS831 alloy by impeding the dislocation movement.

3.3. Load-relaxation behavior

To further investigate the effect of the internal microstructural factors such as dispersoids on elevated temperature deformation behavior, the alloys were investigated within the framework of an internal variable theory [22]. The rheological model of an internal variable theory is shown in Fig. 4. It shows that grain boundary sliding is mainly accommodated by a dislocation process, denoted as grain matrix deformation, giving rise to a recoverable internal strain a and a non-recoverable plastic strain α. Grain boundary sliding and grain matrix deformation can be considered to compete against each other at high temperatures. Considering simple dislocation dynamics, the following stress relationship together with the kinematics relationship among the deformation state variables can be prescribed as,

$$\sigma = \sigma^{\mathrm{I}} + \sigma^{\mathrm{F}}$$
$$\dot{\varepsilon}_{\mathrm{total}} = \dot{a} + \dot{\alpha} + \dot{g} \quad (2)$$

with σ^{I} and σ^{F} denoting the internal stress to overcome a long range interaction force among glide dislocations and the friction stress, respectively. In the strain rate term, $\dot{a}$ means recoverable internal strain tensor, $\dot{\alpha}$ the non-recoverable plastic strain rate and $\dot{g}$ is a strain rate due to grain boundary sliding. At high temperature, the friction stress σ^{F} is generally very small compared

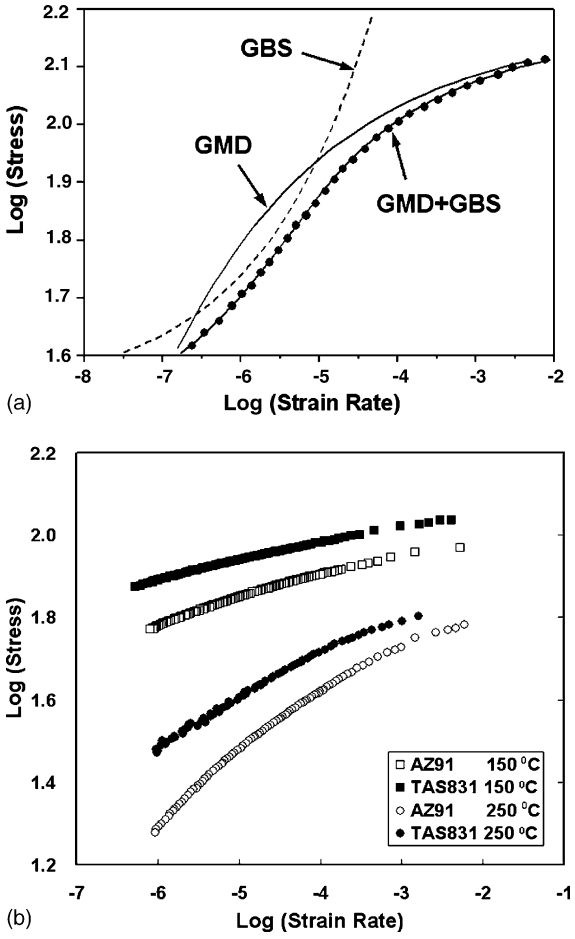

Fig. 5. (a) Schematic and (b) experimental load-relaxation flow curves of the alloys.

to the internal stress σ^{I}. The internal strain tensor $\dot{a}$ can also be neglected. It is therefore sufficient to consider that total strain rate consists of $\dot{\alpha}$ and $\dot{g}$. If the grain boundary sliding is the only deformation mechanism operating (i.e., $\dot{\alpha} \approx 0$), then the plot of Eq. (2) will show the concave curves as schematically shown in Fig. 5a. On the other hand, plot of Eq. (2) will show the convex curves if the grain matrix deformation is the only deformation mechanism operating. Since grain boundary sliding can occur simultaneously with grain matrix deformation, actual flow curves can be shown as composite curves. Based on this internal variable theory, load-relaxation tests were conducted at the temperatures of 150 °C and 250 °C. The flow curves of the alloys obtained from load-relaxation tests are shown in Fig. 5b. It shows that all the flow curves fit well by the grain matrix deformation constitutive relationship. Any noticeable concave portions, the evidence for grain boundary sliding, were not found in all cases. Therefore, during the high temperature load-relaxation test, the deformation of both alloys occurs by grain matrix deformation, not by grain boundary sliding, just like in the case of creep deformation. Since the occurrence of grain boundary sliding is not observed in the present case, data obtained by load-relaxation tests can be considered as representing the deformation process of $\dot{\alpha}$ element only (i.e., grain matrix deformation).

Table 3
Constitutive parameters calculated by internal variable theory

Alloy	Temperature (°C)	σ^*	$\log \dot{\alpha}^*$
AZ91	150	158	−7.3
	250	158	−4.3
TAS831	150	179	−7.1
	250	178	−2.8

From Eq. (3), we can calculate σ^* and $\dot{\alpha}^*$:

$$\sigma = \frac{\sigma^*}{\exp\left(\left(\frac{\dot{\alpha}^*}{\dot{\varepsilon}}\right)^p\right)} \quad (3)$$

where σ^* is an internal strength of the material by internal obstacles which disturbs dislocation movements and $\dot{\alpha}^*$ is a conjugate reference strain rate. Calculated parameters are shown in Table 3. Between two alloys, TAS831 alloy shows a higher value of σ^* than AZ91 alloy, suggesting that the internal obstacles such as thermally stable particles within the matrix of TAS831 alloy increase the internal strength. Lower value of non-recoverable plastic strain rate $\dot{\alpha}^*$ in TAS831 alloy than that in AZ91 alloy can also be explained by the same reason. Activation energies for load relaxation were also calculated. For load-relaxation test, internal plastic strain rate $\dot{\alpha}^*$ was used as a strain rate to calculate the activation energy. By plotting $\log \dot{\alpha}^*$ versus $1/T$, the activation energies for load relaxation can be calculated (Fig. 6). Calculated activation energies for the load relaxation are smaller than those for creep test because only internal factors are considered in this calculation. It shows that the activation energy for TAS831 alloy (80.9 kJ/mol) is much higher than that for AZ91 alloy (55.1 kJ/mol). This result agrees with the above-mentioned result which shows that TAS831 alloy has a higher value of σ^* than AZ91 alloy. Therefore, it can be concluded from the load-relaxation test results that the presence of thermally stable Mg_2Sn particles within matrix of TAS831 alloy improves the resistance to high temperature deformation of TAS831 alloy over that of AZ91 alloy, as exemplified by higher activation energy, higher internal strength and lower strain rate of the former than those of the latter. It is expected that the presence of Mg_2Sn particles within matrix of the TAS831 alloy have a similar effect on its creep resistance.

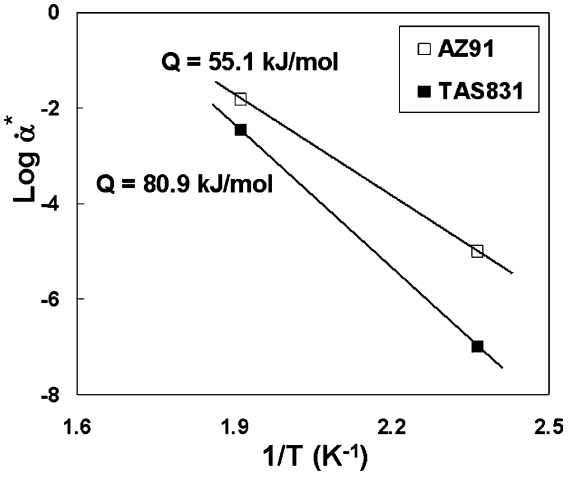

Fig. 6. Plot of $\log \dot{\alpha}^*$ vs. $1/T$ showing the activation energy for load relaxation.

4. Summary

Tensile and creep properties of die cast Mg–Sn–Al–Si (TAS831) alloy were investigated in the present study and major conclusions can be summarized as follows:

(i) The microstructure of TAS831 alloy contains thermally stable Mg_2Sn particles within matrix and along grain boundaries. It also contains a small volume fraction of thermally stable Mg_2Si particles. The presence of these particles in TAS831 alloy is responsible for its improved tensile and creep properties over those of AZ91 alloy.
(ii) It has been shown that the deformation of both TAS831 and AZ91 alloys is controlled by dislocation climb controlled creep based on the analyses of creep behavior and load-relaxation behavior at elevated temperatures. Analyses of elevated temperature deformation behavior in the context of internal variable theory show that the presence of thermally stable dispersoids in TAS831 alloy increases the resistance to grain matrix deformation.

Acknowledgements

This work was partially supported by the National Research Laboratory Program funded by the Ministry of Science and Technology and by the Ministry of Commerce, Industry and Energy of Korea.

References

[1] B.L. Mordike, T. Ebert, Mater. Sci. Eng. A 302 (2001) 37–45.
[2] W. Blum, P. Zhang, B. Watzinger, B.V. Grossmann, H.G. Haldenwanger, Mater. Sci. Eng. A 319–321 (2001) 735–740.
[3] Y.B. Unigovski, E.M. Gutman, Appl. Surf. Sci. 153 (1999) 47–52.
[4] P. Zhang, Scripta Mater. 52 (2005) 277–282.
[5] J.G. Wang, L.M. Hsiung, T.G. Nieh, M. Mabuchi, Mater. Sci. Eng. A 315 (2001) 81–88.
[6] M.S. Yoo, K.S. Shin, N.J. Kim, Metall. Mater. Trans. A 35 (2004) 1629–1632.
[7] M. Vogel, O. Kraft, E. Arzt, Scripta Mater. 48 (2003) 985–990.
[8] B.L. Mordike, T. Ebert, Mater. Sci. Eng. A 302 (2001) 37–45.
[9] M.S. Yoo, Y.C. Kim, S. Ahn, N.J. Kim, Mater. Sci. Forum 419–422 (2003) 419–424.
[10] D.H. Kang, M.S. Yoo, S.S. Park, N.J. Kim, Mater. Sci. Forum 475–479 (2005) 521–524.
[11] D.H. Kang, M.S. Yoo, S.S. Park, N.J. Kim, Mater. Sci. Forum 488–489 (2005) 759–762.
[12] M. Regev, E. Aghion, A. Rosen, M. Bamberger, Mater. Sci. Eng. A 252 (1998) 6–16.
[13] A. Luo, M.O. Pekguleryuz, J. Mater. Sci. 29 (1994) 5259–5271.
[14] L. Lin, Z. Liu, L.J. Chen, F. Li, Met. Mater. Int. 10 (2004) 507–512.
[15] J.J. Kim, D.H. Kim, K.S. Shin, N.J. Kim, Scripta Mater. 41 (1999) 333–340.
[16] C.D. Lee, K.S. Shin, Met. Mater. Int. 9 (2003) 21–27.

[17] D.H. Kang, S.S. Park, N.J. Kim, unpublished research.
[18] S. Spigarelli, E. Cerri, E. Evangelista, L. Kloc, J. Cadek, Mater. Sci. Eng. A 254 (1998) 90–98.
[19] S.S. Vagarali, T.G. Langdon, Acta Metall. 29 (1981) 1969–1982.
[20] A.A. Luo, Int. Mater. Rev. 49 (2004) 13–30.
[21] M.S. Dargusch, G.L. Dunlop, K. Pettersen, Transactions of the 19th International Die Casting Congress, NADCA, Illinois, 1997, pp. 131–137.
[22] W. Bang, T.K. Ha, Y.W. Chang, Mater. Sci. Tech. 18 (2002) 1439–1444.